Linking northeastern North Pacific oxygen changes to upstream surface outcrop variations

Sabine Mecking and Kyla Drushka

5 University of Washington, Applied Physics Laboratory, Seattle, WA, USA

Correspondence to: Sabine Mecking (mecking@uw.edu)

Abstract. Understanding the response of the ocean to global warming, including the renewal of ocean waters from the surface (ventilation), is important for future climate predictions. Oxygen (O_2) distributions in the ocean thermocline have proven

10 an effective way to infer changes in ventilation because physical processes (ventilation and circulation) that supply oxygen are thought to be primarily responsible for changes in interior oxygen concentrations. Here, the focus is on the North Pacific thermocline, where some of the world ocean's largest oxygen variations have been observed. These variations, described as bi-decadal cycles on top of a small declining trend, are strongest on subsurface isopycnals that outcrop into the mixed layer of the northwestern North Pacific in late winter. In this study, surface density time series are reconstructed in this area using observational

15 data only and focusing on the time period from 1982, the first full year of the satellite SST record, to 2020. It is found that changes in maximum annual outcrop area of the densest isopycnals outcropping in the northwestern North Pacific are correlated with interannual oxygen variability observed at Ocean Station P (OSP) downstream at about a 10-year lag. The hypothesis is that ocean ventilation/uptake of oxygen is greatly reduced when the outcrop areas are small and that this signal travels within the North Pacific Current to OSP, with 10 years being at the higher end of transit times reported in other studies. It is also found that sea surface

20 salinity (SSS) dominates over sea surface temperature (SST) in driving interannual fluctuations in maximum annual surface density in the northwestern North Pacific, highlighting the role that salinity may play in altering ocean ventilation. In contrast, SSS and SST contribute about equally to the long-term declining surface density trends that are superimposed on the interannual cycles.

1 Introduction

Ventilation, the renewal of ocean waters from the sea surface, is expected to decrease due to ocean warming and the resulting

25 increases in stratification (Helm et al., 2011; Capotondi et al., 2012; Heinze et al., 2015). During ventilation, water that is transported from the surface mixed layer into the ocean interior also carries along atmospheric gases, including oxygen (O_2) and carbon dioxide (CO_2), that have exchanged between the ocean and the atmosphere while the water was at the surface. A reduction in ventilation has thus also been linked to deoxygenation in the ocean interior (Keeling et al., 2010) and reduced uptake of anthropogenic CO_2 (Heinze et al., 2015; Franco et al., 2021) by the world's oceans. This has impacts on ocean ecosystems because

30 a reduction in O_2 can shift previously well-oxygenated marine environments to hypoxic conditions (Whitney et al., 2007), affecting marine life. A reduction in oceanic CO_2 uptake creates a positive feedback to global warming caused by rising atmospheric CO_2 levels since it leaves more CO_2 in the atmosphere (Friedlingstein, 2015).

The North Pacific thermocline is one of the first regions for which large variations in oceanic O_2 concentrations were observed and

35 linked to ventilation changes (Andreev and Kusakabe, et al., 2001; Emerson et al., 2001; Ono et al., 2001; Watanabe et al., 2001; Emerson et al., 2004). Observations from repeat hydrographic sections have shown that changes between decades can be 20 µmol kg⁻¹ or more in both the eastern and western North Pacific (Mecking et al., 2008; Takatani et al., 2012; Sasano et al., 2015). Fifty

years of time series data from Ocean Station Papa (OSP; 145°W, 50°N) in the Gulf of Alaska in the northeastern North Pacific

(black circle in Figure 1) have indicated that there are bi-decadal O_2 variations that occur on subsurface isopycnals in addition to

40   a smaller declining trend associated with ocean warming (Whitney et al., 2007; Cummins and Ross, 2020). The bi-decadal cycles

in the Gulf of Alaska roughly correspond to oscillations in O_2 and nutrients observed in the western subarctic Pacific (Ono et al.,

2001) with an order 5–10 year lag depending on the density surface (Whitney et al., 2007), likely reflecting the time that it takes

for waters formed in the northwestern North Pacific to travel east with the North Pacific Current.

45
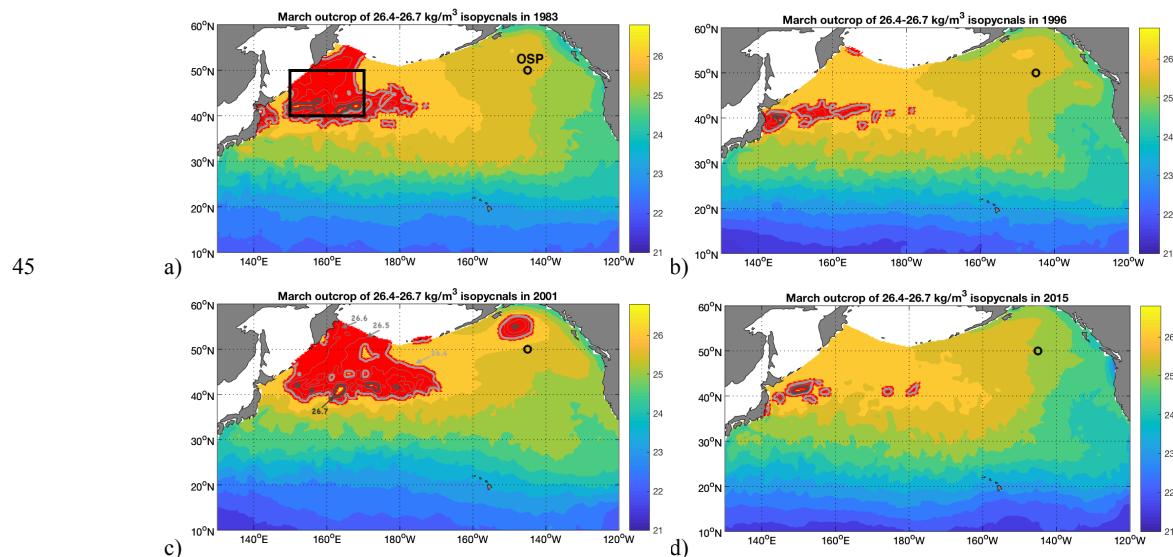
Figure 1. Examples of maxima (left) and minima (right) of March outcrop areas of the σ_θ=26.4-26.7 kg m^{-3} isopycnal range: (a) 1983, (b) 1996,

(c) 2001, and (d) 2015. Dataset used is EN4-OISST: ¼° degree satellite SST combined with EN4 SSS (interpolated to ¼°). Colored contours and

50   colorbar are surface potential density anomaly, with anomalies in the σ_θ=26.4-26.7 kg m^{-3} range indicated with red markers (highlighting the

outcrop area of those isopycnals). The contour lines, as labeled in (c), show the σ_θ=26.4 kg m^{-3} (light gray bold line), σ_θ=26.5 kg m^{-3} and 26.6 kg

m^{-3} (medium gray thin lines), and σ_θ=26.7 kg m^{-3} (dark gray bold line) outcrops. The location of OSP at 145°W, 50°N, as labeled in a), is marked

by an open black circle. The area used for northwestern North Pacific SST, SSS, and surface density averaging, as shown in Figures 6, A1, and

A5–7, is outlined by a black box in (a).

55

The mechanisms responsible for the observed variability in thermocline O_2 content have been investigated in a variety of ways

(Ono et al., 2001; Watanabe et al., 2001; Emerson et al., 2001, 2004; Deutsch et al., 2005; Andreev and Baturina, 2006; Mecking

et al., 2006; Whitney et al., 2007, Crawford and Peña, 2016; Stramma et al., 2020; Sasano et al., 2018). One suggestion is that

surface density variations, particularly variations in the northwest North Pacific late winter outcrop location and area (including

60   complete cessation of outcropping) of the $\sigma_\theta = 26.6$ kg m^{-3} isopycnal, which exhibits some of the largest O_2 variations downstream,

play a key factor (Emerson et al, 2004; Mecking et al., 2006, 2008). However, correlating the O_2 changes with surface forcing

mechanisms, such as temperature and wind stress changes associated with the Pacific Decadal Oscillation (Mantua et al, 1997;

Deser et al.,1999) remains inconclusive (Mecking et al., 2008). Alternatively, as a result of the 18.6-year lunar nodal tidal cycle,

variations in tidal mixing in the narrow passages between the Kuril Islands (45-50°N) separating the open North Pacific from the

65   Sea of Okhotsk may affect surface and near-surface properties in the northwestern North Pacific (Andreev and Baturina, 2006;

Yasuda et al. 2006) and cause the bi-decadal O_2 cycles observed downstream at OSP (Whitney et al., 2007).

While there remain open questions regarding the driving forces of the ventilation changes in the North Pacific (Sasano et al., 2018), it seems clear that surface/mixed layer density variations in the northwestern North Pacific are important, in particular in late

70 winter when the densest isopycnals outcrop, mixed layers are the deepest, and permanent subduction/ventilation (i.e. transport of oxygenated waters from the mixed layer into the thermocline that is not reversed through mixed layer deepening in the next winter season) takes place (Huang and Qui, 1994). Modeling studies (Deutsch et al., 2005, 2006; Kwon et al., 2016) have confirmed what was first suspected from observations (Emerson et al., 2001, 2004): physical processes (gyre ventilation and circulation) are dominant in the North Pacific in producing O_2 variations in the ocean interior, with contributions from changes in biological

75 respiration rates being minor.

In this paper, we zoom in on the northwestern North Pacific, reconstructing surface density time series using observational data only. We focus on the time period from 1982, the beginning of the full annual satellite SST record, to the present. We compare this surface density record to the O_2 time series at OSP in the northeastern North Pacific and examine connections between

80 ventilation changes in the northwest, including the contributions of salinity versus temperature to surface density changes, and O_2 changes downstream. This provides a data-based assessment of the hypothesis that surface density variations are a main driver of O_2 changes in the ocean interior. The data and data methods used are described in section 2, results are discussed in section 3, and summary and conclusions are presented in section 4.

2 Data and Methods

85 ### 2.1 Datasets

As the basis for the surface density calculation, we use the EN4 dataset (version EN4.2.1) that provides quality controlled subsurface ocean temperature and salinity profiles as well as objective analysis of those data on monthly 1°x1° grids with 42 vertical levels from 1900 to the present (Good et al., 2013). EN4 is based on measurements from the World Ocean Database (WOD) as well as from the Global Temperature and Salinity Profile Program (GTSPP, from 1990 onward) and the Argo global

90 data assembly centers (GDACS) from 2000 onward. The data going into EN4 are quality controlled using a series of consistent control steps and then gridded based on an iterative optimal interpolation method, taking into account anomalies (relative to climatology) of prior months' data and providing uncertainty estimates (Good et al., 2013). Here, we utilize the version of EN4 with the Gouretski and Reseghetti (2010) bias correction, though the findings are insensitive to the choice of corrections available with the EN4 data. We use the upper level of the EN4 temperature and salinity fields that are nominally at 5 m depth and refer to

95 them as sea surface temperature (SST) and salinity (SSS) for brevity.

In addition to SST from EN4, we also use SST data from the NOAA Optimal Interpolation SST (OISST) Version 2 High Resolution product (Reynolds et al., 2007, Banzon et al., 2016). The OISST V2 product is based on a blend of satellite and in situ observations, and is available on a global 1/4°x1/4° grid from September 1981 onward. We average daily fields to produce monthly SST maps,

100 using data from 1982 to 2020. Comparisons with SST from EN4 enable us to examine effects of spatial resolution on surface density patterns.

Satellite salinity data have only been available since 2009 (European SMOS satellite, 2009–present; U.S. Aquarius satellite, 2011–2015; U.S. SMAP satellite, 2015–present). An optimally-interpolated multi-satellite salinity product that combines data from all

105   three satellites and includes bias corrections based on in-situ data (Melnichenko et al., 2021) compares well to EN4 with nearly identical salinity averages in the northwestern North Pacific (Figure A1), but is not used for this study due to its relatively short duration (2011–present). Thus, we instead combine the OISST data with EN4 SSS data (interpolated to 1/4°x1/4°) to obtain surface density fields at higher resolution than EN4 alone, acknowledging the caveat that any small-scale density variability observed is a result of SST patterns only. We refer to this dataset as EN4-OISST. The TEOS-10 scale is used to compute surface potential density

110   from SST and SSS for both the EN4 and EN4-OISST datasets using the Gibbs Seawater toolbox (McDougall and Barker, 2011).

To examine ocean interior oxygen variations, we use data from OSP (145°W, 50°N), which provides one of the longest data timeseries in the world's ocean, with weather ship data available since 1956 (Whitney et al., 2007; Cummins and Ross, 2020; Ross et al., 2020). Currently, OSP is occupied ~3 times per year as part of the Canadian Line-P hydrographic cruises from Vancouver

115   Island to OSP. Cruise data is publicly available from the Fisheries and Oceans Canada database (Freeland, 2007; Whintey et al., 2007), where we downloaded the OSP bottle data from 1956 until 2020. For the calculation of vertical profiles of potential density at OSP, in situ temperature and salinity were converted to conservative temperature and absolute salinity using the TEOS-10 scale (McDougall and Barker, 2011), and the OSP oxygen data were then mapped onto a potential density anomaly-time grid using standard objective mapping techniques (Bretherton et al., 1976; Roemmich, 1983). To put the OSP timeseries data into spatial

120   context, we also examine repeat hydrography data (vertical sections of temperature, salinity, and oxygen; Talley et al., 2016) from the northeastern North Pacific. The most recent P16N section, a key U.S. repeat section along 152°W (Emerson et al., 2004; Mecking et al., 2008) that is re-occupied every ten years or so, was occupied in 2015 as part of the Global Ocean Ship-based Hydrographic Investigations Program (GO-SHIP), and the P1 section along 47°N (Watanabe et al., 2001; Emerson et al., 2004), also covering parts of the northeastern North Pacific, was occupied in its full extent as part of the Japanese contribution to GO-

125   SHIP in 2014 (Figure A2).

2.2 Outcrop area as ventilation metric

Variations in surface potential density are examined, based on the EN4-OISST dataset, using the outcrop area of the densest isopycnals to outcrop in the northwestern North Pacific in March (σ_θ=26.4-26.7 kg m^{-3}) as a metric (Figure 1). These isopycnals are chosen because they encompass the isopcynal where the largest North Pacific O$_2$ changes have been observed (σ_θ=26.6 kg m^{-3}

130   ^{3}; Emerson et al., 2004) and because they mark the bottom of the ventilated thermocline. If they stop outcropping or if the outcrop area is reduced, it can be assumed that ventilation, including transport of oxygen from the surface mixed layer on these density surfaces into the ocean interior, is also stopped or reduced during that time (Mecking et al., 2008). Using late winter data (March) is important because this is when surface waters become the densest and permanent subduction from the mixed layer along outcropping isopycnals takes place, renewing waters in the deepest part of the ventilated thermocline (Huang and Qiu, 1994).

135   While vertical Ekman pumping and lateral induction estimates are needed to fully quantify the amount of water that is transported across the base of the mixed layer, the spatial extent of the surface outcrop area can be used as a proxy for the amount of ventilation taking place, with a larger outcrop area indicating more ventilation and a smaller outcrop area indicating less ventilation (Mecking et al., 2008; Kwon et al., 2016). Since the OISST product represents temperature at the ocean surface, our outcrop area calculations based on EN4-OISST (and also EN4) rely on surface density rather than density at the base of the mixed layer where the subduction takes place. We note that surface densities are slightly lower than densities at the base of the mixed layer (by ~0.03 kg m^{-3} for

140   individual profiles; Holte and Talley, 2009), but are expected to represent temporal variations in outcrop area accurately. For the purpose of this paper, the terms surface and mixed layer density are used interchangeably.

3. Results

3.1 Temporal variations in outcrop area of densest outcropping isopycnals

145   The surface outcrop areas of the σ_θ=26.4-26.7 kg m^{-3} isopcynals in March show large interannual differences (Figure 1; red symbols). The σ_θ=26.7 kg m^{-3} isopycnal (dark gray bold lines in Figure 1) reaches the surface in the years of maximum outcrop areas (e.g. 1983, 2001; Figure 1a, c) as well as the years of minimum outcrop areas (e.g. 1996, 2015; Figure 1b, d), though barely. However, the strong fluctuations in March outcrop area of σ_θ=26.4-26.7 kg m^{-3} are caused mostly by changes in the outcrop location of the lighter isopcynals (σ_θ=26.4-26.6 kg m^{-3}), as can been seen for example by large variations in the σ_θ=26.4 kg m^{-3} outcrop

150   (light gray bold line in Figure 1) that can extend significantly to the east of the dateline in high outcrop area years. In 1983 (Figure 1a) and 2001 (Figure 1c) the σ_θ=26.4-26.7 kg m^{-3} outcrop area forms a large, continuous patch extending from east of Japan to east of the dateline and between ~40°N and the Bering Sea (area 2.47x10^6 km^2 and 3.58x10^6 km^2, respectively). In contrast, in 1996 (Figure 1b) and 2015 (Figure 1d) this area is contracted to small disjointed outcrop patches along 40°N (area 0.592x10^6 km^2 and 0.305x10^6 km^2, respectively), allowing for very little ventilation. A timeseries of the monthly σ_θ=26.4-26.7 kg m^{-3} outcrop area in

155   the North Pacific for all years from 1982 to 2020 (blue line; Figure 2) illustrates that 1) the outcrop area is the indeed largest in March of each year since the isopycnals in this density range all reach the surface then, and 2) that there are distinct March minima in 1995-1997, 2011, and 2014-2015 (area <10^6 km^2), compared to the March outcrop area in the years before/after, and a distinct March maximum in particular in 2001 (area >3.5x10^6 km^2). Uncertainties in the March outcrop areas that are calculated based on the salinity and temperature uncertainties reported with the EN4 dataset (Good et al, 2013) using a Monte Carlo approach are 1-2

160   magnitudes smaller than the outcrop areas (not shown), indicating that the large interannual changes in outcrop area are significant.
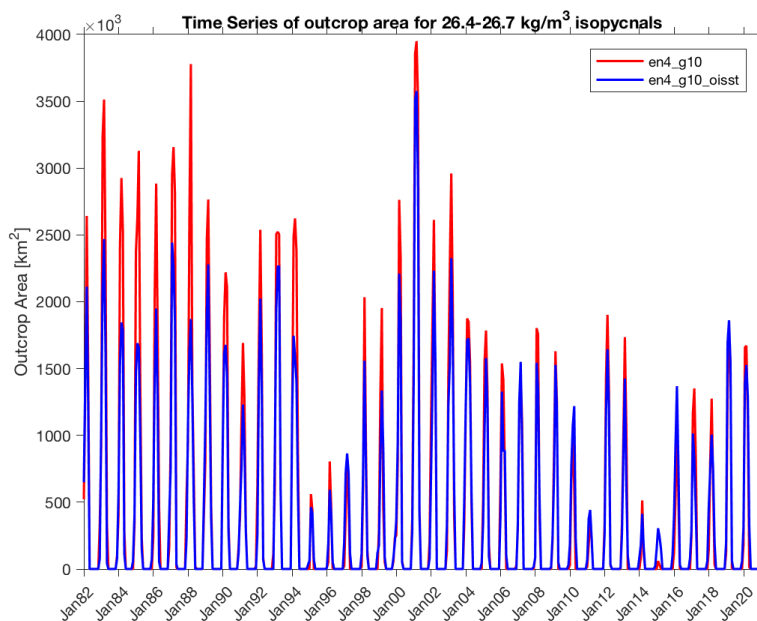
Figure 2. Time series of surface outcrop area of σ_θ=26.4-26.7 kg m^{-3} in the North Pacific. Blue line is based on surface density from the 1/4°
165   EN4-OISST data set, and red line is based on surface density from the 1° smoothed EN4 dataset. The peaks in outcrop area occur just after January (shown on the x-axis), usually in March, of each year.

To assess how spatial resolution of data and small-scale variability affects the results, we compare EN4-OISST with the lower-resolution EN4 dataset (1°x1°) that is based on EN4 temperature and salinity (section 2.1). The time series of the σ_θ=26.4-26.7 kg

170   m^{-3} outcrop area from 1982 to 2020 using EN4 (red line; Figure 2) exhibits larger March peak values than the EN4-OISST data set (blue line; Figure 2) in almost every year, likely because SST fields in EN4 are more smoothed and less patchy than the OISST satellite product. But the EN4-derived outcrop areas show the same pattern of maxima and minima as EN4-OISST, indicating that in particular the extreme minima in 1995-1997, 2011, and 2014-2015 and the extreme maximum in 2001 are a robust result. The EN4-OISST and EN4 datasets (Figure 2), despite the 2001 maximum, also both show a declining trend in the σ_θ=26.4-26.7 kg m^{-}

175   ^{3} outcrop area from 1982–2020 that is discussed further in the next section. We continue to use the EN4-OISST dataset for the remainder of the analysis given its higher resolution, knowing that the trends and overall patterns in outcrop area are consistent among the higher and lower resolution datasets.

3.2 Correlations between outcrop area and O$_2$ timeseries

180   Since OSP is downstream of the σ_θ=26.4-26.7 kg m^{-3} outcrop area in the northwest Pacific (as indicated by streamlines on σ_θ=26.6 kg m^{-3} in Figure A2), O$_2$ distributions observed at OSP, mapped onto a potential density anomaly-time grid (Section 2.1), are expected to be affected by O$_2$ uptake variability (i.e., ventilation variability) in the isopycnal outcrop region. For the OSP data, we confirm that there are large decadal variations in O$_2$ concentration (Whitney et al., 2007; Cummins and Ross, 2020) on isopycnals near the bottom of the ventilated thermocline (Figure 3a) where maximum O$_2$ variability, based on repeat hydrography data, has

185   been observed previously on the $\sigma_\theta \cong 26.6$ kg m^{-3} isopycnal (Mecking et al., 2008). Figure 3b illustrates that densities around σ_θ=26.6 kg m^{-3} are also the isopycnals where the largest decadal variations (and long-term O$_2$ trends) occur at OSP, as indicated by overall maxima in standard deviation and negative trend of O$_2$ over the time period of the OSP record (1956-2020) around σ_θ=26.5-26.7 kg m^{-3}. Maxima in declining O$_2$ trends at OSP have also been reported in this density range by Whitney et al., (2007; σ_θ=26.5 kg m^{-3}) and Crawford and Peña (2016; σ_θ=26.7 kg m^{-3}), each using slightly different methodologies, but also slightly

190   deeper on σ_θ=26.8 kg m^{-3} (Cummins and Ross, 2020) which does not outcrop in the North Pacific, solidifying that this is the density range of largest O$_2$ decline or close to it in the northeastern North Pacific. Combining the O$_2$ data on σ_θ=26.6 kg m^{-3} with the timeseries of annual maximum σ_θ=26.4-26.7 kg m^{-3} outcrop area from the EN4-OISST dataset (maxima in blue line each year in Figure 2), which we use as a proxy for ventilation of the isopycnals at the bottom of the ventilated thermocline, shows that a strong minimum in O$_2$ in 2005–2007 lags the minimum in annual maximum outcrop area in 1995–1997 by about a decade (Figure 4; solid

195   blue/cyan versus red/magenta lines). Such a lag is expected, assuming it takes about 10 years for surface waters from the outcrop area in the northwestern North Pacific to reach OSP on this isopycnal (Whitney et al., 2007). This transit time is somewhat larger than the 7–8 year west-to-east transit time estimated by Ueno and Yasuda (2003) on σ_θ=26.7 kg m^{-3} from a North Pacific inverse model, but given the differences in data and methods used, we consider our transit time estimate to be roughly consistent with Ueno and Yasuda's.

200
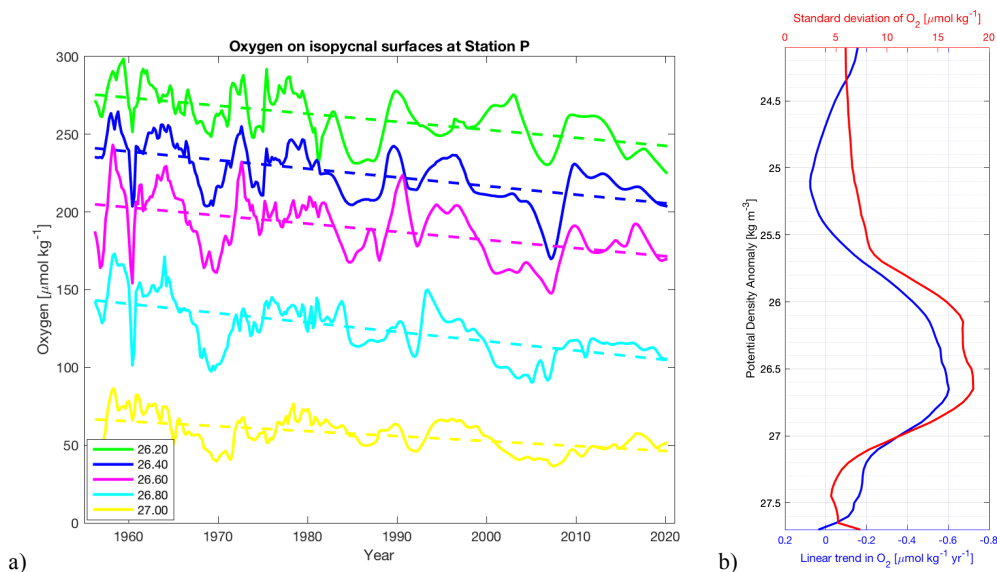
Figure 3. (a) Timeseries of O_2 at OSP (see location in Figure 1) on isopycnals from σ_θ=26.2-27.0 kg m^{-3} (in 0.2 kg m^{-3} increments). Linear trend of O_2 on each isopycnal is shown as a dashed line. (b) Isopycnal profile of the linear O_2 trend (blue) and the standard deviation of the O_2 variations (red) on isopycnals (in 0.05 kg m^{-3} increments) at OSP. The vertical profiles were smoothed with a 9-point running average (corresponding to a 0.4 kg m^{-3} averaging interval). Data used are objectively mapped OSP data.

Estimation of lagged correlations between O_2 on σ_θ=26.6 kg m^{-3} and the annual maximum σ_θ=26.4-26.7 kg m^{-3} outcrop area, using the unfiltered timeseries (solid blue/red lines in Figure 4) as well as filtered data (solid cyan/magenta lines in Figure 4), also results in the best correlation at a 10-year lag for the O_2 record lagging annual maximum outcrop area (r=0.50 for filtered, detrended data; Figure 5). Note that the correlation is even better for O_2 leading the annual maximum outcrop area (r=0.59 at a –10-year lag for O_2; Figure 5), which is unphysical since O_2 in the interior ocean does not have an obvious effect on surface density. However, since the O_2 variations and possibly the annual maximum outcrop area are associated with bi-decadal cycles, shifting O_2 either forward or backward in time by 10 years should result in a strong correlation with the outcrop area. This also explains why there is a maximum negative correlation at a close to zero lag (r=–0.65, Figure 5).

In addition to decadal scale variability, both the OSP O_2 timeseries on σ_θ=26.6 kg m^{-3} and the northwestern North Pacific maximum annual outcrop area (Figure 4) exhibit declining long-term linear trends amounting to –0.53 µmol kg^{-1} yr^{-1} and –2.45 x 10^{10} m^2 yr^{-1}, respectively (dashed lines in Figure 4). Previous studies have shown that there is a long-term decrease in O_2 at OSP (Whitney et al., 2007; Stramma et al, 2020) as well as in surface density in the northwestern North Pacific (Ono et al., 2001; Durack and Wijffles, 2010), the latter of which is consistent with the decreasing trend in outcrop area of the densest outcropping isopycnals (σ_θ=26.4-26.7 kg m^{-3}) that we have shown here. The trends in O_2 and outcrop area likely occur together for the same reasons that the decadal scale variability in O_2 at OSP and outcrop area are correlated (with O_2 lagging; see previous paragraph): as the outcrop area of the σ_θ=26.4-26.7 kg m^{-3} isopycnals declines, less ventilation of these isopycnals takes place and less O_2 is transported from the mixed layer into the ocean interior, causing the declining trend in O_2 on those isopycnals at OSP.
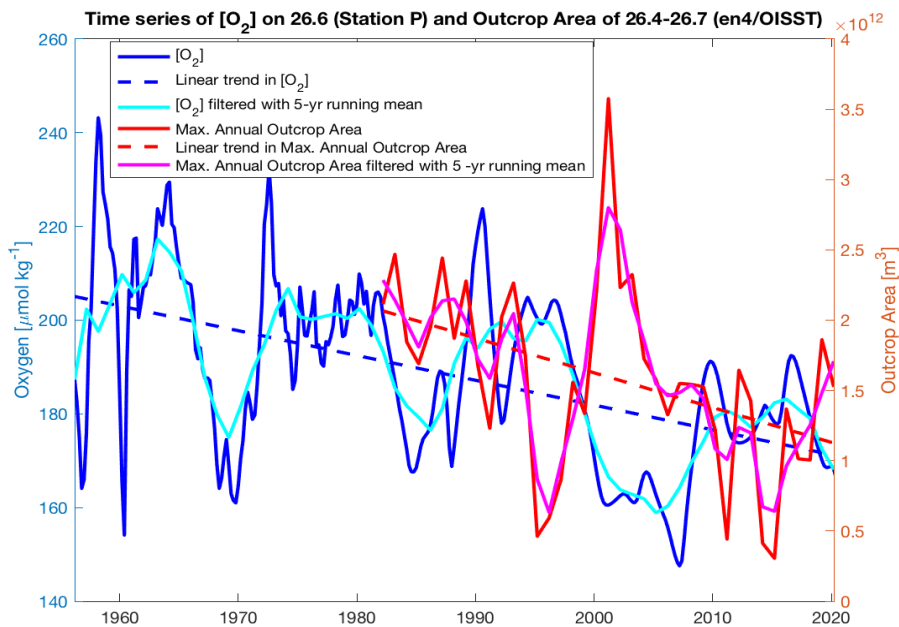
Figure 4. Timeseries of annual maximum outcrop area of σ_θ=26.4-26.7 kg m^{-3} based on EN4-OISST data set (Figure 2) and of O$_2$ on σ_θ=26.6 kg m^{-3} at OSP (Figure 3a) plotted on top of each other (solid red and blue lines, respectively). Also shown are the data filtered with a 5-year running mean (solid cyan and magenta lines, respectively) and the linear trends (dashed red and blue lines, respectively) in each time series. The linear trends are –2.45 x 10^{10} m^2 yr^{-1} for the outcrop area timeseries and –0.53 μmol kg^{-1} yr^{-1} for the O$_2$ timeseries.
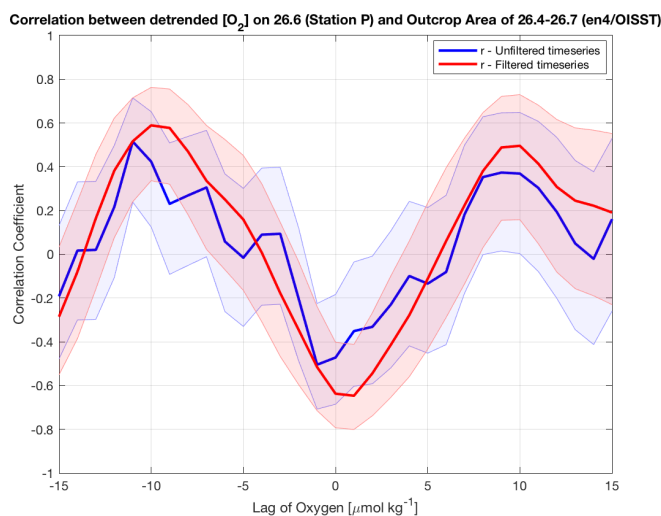
235

Figure 5. Lagged correlations between detrended timeseries of maximum annual outcrop area of σ_θ=26.4-26.7 kg m^{-3} and of O$_2$ on σ_θ=26.6 kg m^{-3} at OSP (solid lines in Figure 4 with linear trend, the dashed line in Figure 4, removed), using unfiltered timeseries data (blue line) and timeseries data filtered with a 5-yr running mean (red line). The x-axis in both panels represents the lag of the O$_2$ timeseries relative to the outcrop area timeseries. Shaded areas show 95% confidence intervals. Maximum correlation values (r) for the filtered data are 0.59 at a –10-yr lag and 0.50 at a +10-yr lag, maximum negative r-value (-0.65) occurs at close to a 0-yr lag.

One caveat to the interpretation of the OSP O_2 data in combination with the northwestern North Pacific outcrop area timeseries comes from repeat hydrography data in the area of OSP (Figure A2). Near the longitude and latitude of OSP (145°W, 50°N), respectively, CLIVAR/GO-SHIP repeat hydrography section differences show continued O_2 decline from the mid-2000s to mid-2010s along 152°W (P16N: 2015 minus 2006; Figure A3a) and 47°N (P1: 2014 minus 2007; Figure A3b), contrary to the OSP data, which indicate an increase in O_2 on the σ_θ=26.4 to 27.0 kg m^{-3} isopycnals between those points in time (Figure 3a). To resolve this, we combine O_2 values from the CLIVAR/GO-SHIP as well as earlier WOCE sections, averaged zonally on isopycnals over the intervals 40-45°N for P16N and 140-165°W for P1 (intervals shown as black lines in Figure A3), with the OSP timeseries directly (Figure A4). This indicates that (1) the section averages for both P16N (Figure A4a) and P1 (Figure A4b) may lead the OSP time series by 2–4 years, suggesting that O_2 signals arrived at the hydrographic section locations a few years earlier than at OSP, and that (2) the repeat hydrography, due to lack of time resolution, does not fully resolve the temporal variability in the O_2 record and misses for example the large O_2 minimum observed at OSP in 2007 that leads the 2010s increase in O_2. While the 2–4 year lead of the section data is larger than one might expect given the proximity of the sections to OSP, we conclude that the repeat hydrography data (within the limits of decadal observations) are still roughly consistent with the OSP data in terms of observed O_2 changes.

3.3 Causes

3.3.1 SSS and SST variability

As outlined in the previous section (3.2), variability in oxygen at OSP in the eastern North Pacific can be explained in part by upstream fluctuations in isopycnal outcrop areas in the northwestern North Pacific with a lag of about 10 years (Figures 4, 5). Here, we assess the drivers of the outcrop area fluctuations by examining the effects of SST and SSS in the northwestern North Pacific (averaged over 40-50°N, 150-170°E; see box in Figure 1a) on surface density (Figure 6). Contributions of SST and SSS (Figure 6a) to annual maximum surface density changes in this area (Figure 6b) are estimated by determining the annual mean cycle of each from the EN4-OISST dataset (also averaged over 40-50°N, 150-170°E) and then calculating surface density with either SST or SSS fixed (at its annual mean cycle) while allowing the other variable to vary (thin solid lines in Figure 6a).

The SSS at the time of maximum annual surface density (late winter; bold red line in Figure 6a) show minima around 1996, 2011, and 2015. These match the years when the annual maximum σ_θ=26.4-26.7 kg m^{-3} outcrop area has minima (Figure 2) and annual maximum surface densities are the lowest (bold black line in Figure 6b). Varying SSS and keeping SST fixed at its annual mean cycle results in annual maximum surface densities (red dashed line in Figure 6b) that follow the annual maximum surface density (bold black line) closely, which indicates that SSS variations are the main driver of interannual variations in annual maximum surface density in the northwestern North Pacific. This includes a rebound to higher surface densities in recent years that is evident in both the total and the SSS-driven density records (Figure 6b) and that is caused by the increase in SSS since 2017 (Figure 6a). In contrast, varying SST and keeping SSS fixed at its annual mean cycle causes much smaller interannual variations in the annual maximum surface density (blue dashed line in Figure 6b) than observed in the full record (bold black line), affirming the lesser role that SST plays in producing the interannual annual maximum surface density variations in the northwestern North Pacific.
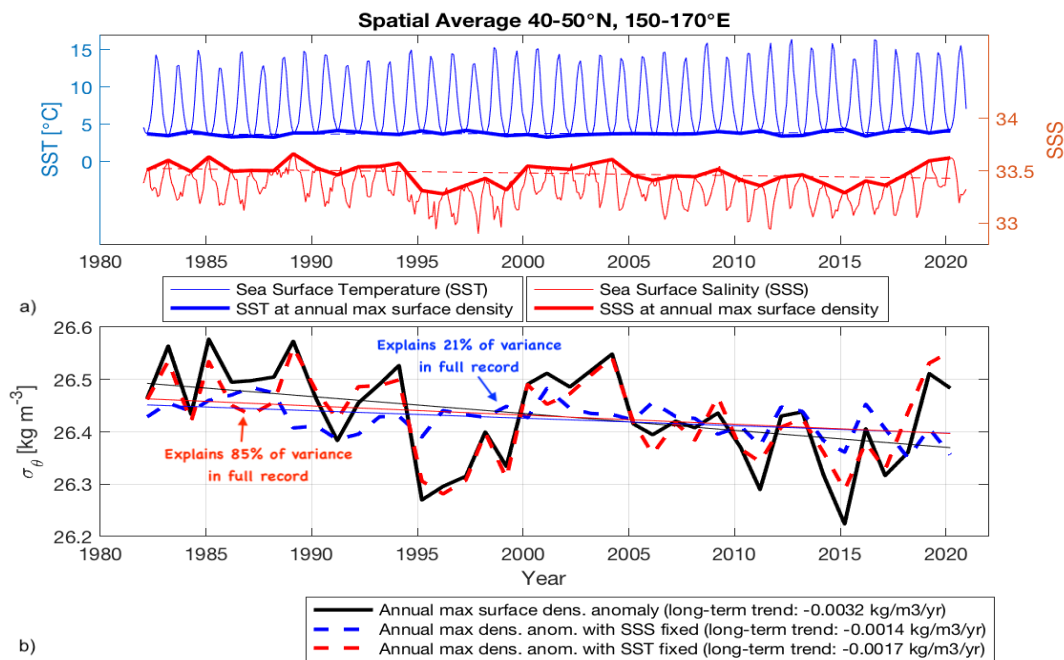
280

Figure 6. (a) SST (bold blue line) and SSS (bold red line) at annual maximum surface density, and (b) annual maximum surface density anomaly (bold black line) and contributions from SST (blue dashed line; with SSS fixed at mean annual cycle during density calculation) and SSS (red dashed line; with SST fixed at mean annual during density calculation) in the northwestern North Pacific (averaged over 40–50°N, 150–170°E; see Figure 1a for area). The red dashed line (SST fixed) and blue dashed line (SSS fixed) explain 85% and 21% of variance of the full record (bold black line), respectively. Linear trends (dashed lines in (a) and thin solid lines in (b), using respective colors) are also shown. Thin solid lines in (a) represent monthly SST and SSS values. Dataset used is the EN4-OISST dataset.

285

Quantitatively, SSS-driven (SST fixed) and SST-driven (SSS fixed) density variability can explain 85% and 21%, respectively, of the variance in total annual maximum surface density in Figure 6b. The contributions do not add up to 100% exactly due to the

290 non-linearities in the calculation of density (equation of state), but it is clear that SSS variations have a much larger contribution (about four times). The dominance of salinity over temperature in driving density fluctuations is consistent with the relatively large haline contraction coefficient compared to the thermal expansion coefficient at this latitude, which govern the contributions of salinity and temperature, respectively, to density (McDougall and Barker, 2011). In terms of long-term linear density trends (thin solid lines in Figure 6b), the SSS-based trend (thin red line, -0.0014 kg m^{-3} y^{-1}) and the SST-based trend (thin blue line, -0.0017

295 kg m^{-3} y^{-1}) contribute about equally to the linear decrease in total annual maximum surface density (thin back line, -0.0032 kg m^{-3} y^{-1}), indicating that long term surface freshening and warming in the northwestern North Pacific are of similar importance in explaining declining surface densities.

Evidence that SSS variations in the northwestern North Pacific are occurring and playing a major role in determining interannual

300 changes in upper ocean density and related ventilation also comes from a study by Uehara et al (2014), who found upper layer (0-100m) salinity variability in the western subarctic gyre (WSG; their Figure 4) similar to the SSS variability reported here (Figure 6a), with our averaging area (see box in Figure 1a) encompassing the southern half of their WSG definition. The time period examined in Uehara et al. (2014) is 1950 to 2008, overlapping the time period of our surface time series (1982–2020) by 26 years and showing the strongest surface salinity freshening signals in the WSG in the early 1960s and in the late 1990s, with the latter

305 corresponding to the SSS minimum we find around 1996 (Figure 6a) and the strong reduction in March outcrop area of σθ=26.4-

26.7 kg m^{-3} from 1995–1997 (Figure 2). Uehara et al. (2014) attribute the upper ocean salinity changes in the WSG to changes in atmospheric forcing such as precipitation and wind, and suggest that these changes are propagated downstream by surface currents into the Bering Sea, the East Kamchatka region, the eastern Sea of Okhotsk and finally the shelves in the northwestern Sea of Okhotsk (see pathways in their Figure 9) where dense shelf waters are formed due to surface cooling. Along this path, mixing
310 variability associated with the 18.6-year nodal tidal cycle, which has been quoted by several authors as a source of upper ocean variability in the northwestern North Pacific especially around the narrow passages in the Kuril Straits that separate the Sea of Okhotsk from the northwestern North Pacific (Yasuda et al. 2006; Whitney et al., 2007; Osafune and Yasuda, 2013; Stramma et al., 2020), may affect upper layer salinities (Uehara et al., 2014). Based on the finding by Uehara et al. that the WSG is at the upstream end of this surface water pathway, however, we conclude that the SSS and outcrop area variability in the northwestern
315 North Pacific reported here (as well as the associated ocean interior O_2 changes at OSP in the northeast) are also due to atmospheric forcing changes rather than the nodal tidal cycle as has been speculated (Whitney et al., 2007). Nevertheless, there could be feedback loops from the dense shelf waters produced in the Sea of Okhotsk at the downstream end of this path back to the surface waters in the open northwestern North Pacific.

320 **3.3.2 Climate indices (PDO, NPGO, and NPI)**

The Pacific Decadal Oscillation (PDO) is the dominant mode of variability in the North Pacific Ocean, with the PDO index defined as the leading principal component of monthly SST variability north of 20°N (Mantua et al. 1997). Since much of the variability in maximum annual surface density that we associate with fluctuations in the σ_θ=26.4-26.7 kg m^{-3} outcrop area and O_2 downstream appear to be driven by salinity variations, as illustrated in the previous section (3.3.1), a correlation between surface density and
325 the PDO is not necessarily expected. Indeed, we find that the correlation between the PDO and annual maximum surface density (averaged over 40-50°N, 150-170°E) timeseries (Figure A5) is only 0.03. There are periods where the two time series seem to be tracking each other (1999–2005), but also several where they clearly show opposite variations (e.g. 1995–1999, 2013–2018), resulting in a correlation close to zero.

330 Only somewhat higher correlations exist between the annual maximum surface density and the North Pacific Gyre Oscillation index (DiLorenzo et al., 2008) and the North Pacific Index (NPI; Trenberth and Hurrell, 1994) with r-values of 0.16 (Figure A6) and 0.14 (Figure A7), respectively, suggesting that these indices also describe little of the surface density variability that drives downstream O_2 variations at OSP. The NPGO index is defined as the second dominant mode of sea surface height (SSH) anomaly variability in the northeastern North Pacific (DiLorenzo et al., 2008) whereas the NPI represents area-weighted winter time sea
335 level pressure over the northern North Pacific (30°N-65°N, 160°E-140°W), which indicates changes in atmospheric circulation. Note that correlations between climate indices and North Pacific thermocline O_2 changes have also been analyzed in different ways (Andreev and Kusakabe, 2001; Ono et al., 2001; Mecking et al., 2008; Stramma et al, 2020), with connections between OSP O_2 and the PDO (Mecking et al., 2008; Stramma et al., 2020) as well as the NPGO (Stramma et al., 2020) found to be weak or inconclusive, but that we focus here on the correlations of climate indices with northwest North Pacific surface density changes
340 because we are evaluating surface density changes as a driving force for OSP O_2 changes in this paper. However, given the dominance of SSS in driving maximum annual surface density changes and the relatively low correlations between the surface density changes and the PDO, NPI or NPGO, we conclude that a climate index that better incorporates salinity is needed.

4. Summary and Conclusions

Analysis of annual maximum outcrop areas of the densest isopycnals to reach the surface in the northwestern North Pacific in
345   winter indicates that there are significant interannual variations as shown by the timeseries of the σ_θ=26.4-26.7 kg m^{-3} outcrop area
in the EN4-OISST dataset staring in 1982 (Figure 2). We consider the size of these outcrop areas as an indicator of how much
ventilation is occurring at the bottom of the ventilated in the North Pacific since renewal of interior waters from the mixed layer
and uptake of gasses only occurs when isopycnals outcrop. A significant 10-year lagged correlation exists between the σ_θ=26.4-
26.7 kg m^{-3} outcrop area variations and the ~bidecadal O_2 cycles at OSP in the northeastern North Pacific that exhibit the largest
350   variability within this density range, giving support to the hypothesis that surface density variations are a main driver of O_2 changes
in the ocean interior. This is consistent with the finding by Sasano et al. (2018) that ventilation variability is a key process for
generating O_2 trends and oscillations on isopycnals that outcrop in the North Pacific (σ_θ<26.8; see their Figure 11). The 10-yr lag
corresponds approximately to the travel time of newly ventilated (and oxygenated) waters from the isopycnal outcrop locations in
the northwestern North Pacific to OSP in the northeast where the isopycnals have descended to the subsurface. Kwon et al. (2016)
355   found similar connections between isopycnal outcropping and ocean interior O_2 changes using the SODA model whereas the
results here are entirely data-based.

A new finding in our analysis is the dominance of SSS over SST in driving interannual fluctuations in annual maximum surface
density (a ventilation proxy similar to annual maximum σ_θ=26.4-26.7 kg m^{-3} outcrop area) in the northwestern North Pacific, as
360   shown in Figure 6b. Evidence that SSS variations in the northwestern North Pacific are occurring and play a major role in
determining interannual changes in upper ocean density and the related ventilation also comes from the analysis of SSS of shelf
waters in the adjacent Sea of Okhotsk (Uehara et al., 2014). In contrast, SSS (freshening) and SST (warming) contribute about
equally to the long-term declining density trends in the northwestern North Pacific (Figure 6b) that are the cause of the long-term
linear decline in σ_θ=26.4-26.7 kg m^{-3} outcrop area and subsequently O_2 concentrations at OSP (Figure 4) as well.
365
In contrast to Kwon et al. (2016), we do not find a good correlation between annual maximum surface density (or outcrop area)
and thus ventilation and the PDO or other climate indices (NPGO, NPI). This may be because the analysis in this paper is using
independent data sets and not a model, where forcing and ocean response are consistent by design. But given the dominance of
SSS in determining interannual variations in surface density, a correlation with PDO (which is based on SST) is not necessarily
370   expected. While it is beyond the scope of this paper, we suggest for future work the development of a North Pacific climate index
that captures the SSS variability as well as expansion of this work to include data-based subduction rates.

Data availability

The data used in this paper are available at the following web-sites:
EN4 - https://www.metoffice.gov.uk/hadobs/en4/
375   OISST - https://www.ncdc.noaa.gov/oisst
OISSS - https://podaac.jpl.nasa.gov/dataset/OISSS_L4_multimission_7day_v1
OSP - www.waterproperties.ca/linep/
CLIVAR/GO-SHIP sections - https://cchdo.ucsd.edu/products/goship-easyocean
PDO - https://www.ncei.noaa.gov/pub/data/cmb/ersst/v5/index/ersst.v5.pdo.dat
380   NPI - https://climatedataguide.ucar.edu/climate-data/north-pacific-np-index-trenberth-and-hurrell- monthly-and-winter

NPGO - http://www.o3d.org/npgo/

World Ocean Atlas climatology - https://www.ncei.noaa.gov/products/world-ocean-atlas

Author contributions

SM and KD designed the study and wrote the manuscript. SM was the project lead and made all the figures in the manuscript.
385 KD was the lead on analyzing the satellite data and combining them with other data products.

Competing interests

The authors declare that they have no conflict of interest.

Acknowledgments

This work was supported by NSF grant OCE-1851149. We would like to thank Roberta Hamme and Tetjana Ross for comments
390 on a draft version of this paper and Fisheries and Oceans Canada for making the OSP data publicly available.

References

Andreev, A. G. and V. I. Baturina, 2006. Impacts of tides and atmospheric forcing variability on dissolved oxygen in the subarctic North Pacific. *J. Geophys. Res.*, 111, C07S10, doi: 10.1029/2005JC003103.

Andreev, A. G. and M. Kusakabe, 2001. Interdecadal variability in dissolved oxygen in the intermediate water layer of the Western
395 Subarctic Gyre and Kuril Basin (Okhotsk Sea), *Geophys. Res. Lett.*, 28(12), 2453-2456.

Banzon, V., T. M. Smith, T. M. Chin, C. Liu, and W. Hankins, 2016. A long-term record of blended satellite and in situ sea-surface temperature for climate monitoring, modeling and environmental studies, *Earth Syst. Sci. Data*, 8, 165–176, doi:10.5194/essd-8-165-2016.

Bretherton, F. P., R. E. Davis, and C.B. Fandry, 1976. A technique for objective analysis and design of oceanographic experiments
400 applied to MODE-73, *Deep Sea Research and Oceanographic Abstracts*, 23 (7), 559-582, https://doi.org/10.1016/0011-7471(76)90001-2.

Capotondi, A., M. A. Alexander, N. A. Bond, E. N. Curchitser, and J. D. Scott, 2012. Enhanced upper ocean stratification with climate change in the CMIP3 models, *J. Geophys. Res.*, 117, C04031, doi:10.1029/2011JC007409

Crawford, W. R., and M. A. Peña, 2016. Decadal trends in oxygen concentration in subsurface waters of the northeast Pacific
405 Ocean. Atmosphere-Ocean, 54:2, 171-192, doi: 10.1080/07055900.2016.1158145.

Cummins, P. F., and T. Ross, 2020. Secular trends in water properties at Station P in the northeast Pacific: An updated analysis, *Prog. Oceanogr.*, 186, 102329, https://doi.org/10.1016/ j.pocean.2020.102329.

Deser, C., M. A. Alexander, and M. S. Timlin, 1999. Evidence for a wind-driven intensification of the Kuroshio Extension from the 1970s to 1980s, *J. Climate*, 12, 1697-1706.

410 Deutsch, C, S. Emerson, and L. Thompson, 2005. Fingerprints of climate change in North Pacific oxygen. *Geophys. Res. Lett.*, **32**, L16604, doi:10.1029/2005GL023190.

Deutsch C., S. Emerson, and L. Thompson, 2006. Physical-biological interactions in North Pacific oxygen variability. *J. Geophys. Res.*, 111, C09S90, doi:10.1029/ 2005JC003179.

Di Lorenzo, E., N. Schneider, K. M. Cobb, P. J. S. Franks, K. Chhak, A. J. Miller, J. C. McWilliams, S. J. Bograd, H. Arango, E.
415 Curchitser, T. M. Powell, and P. Rivière, 2008. North Pacific Gyre Oscillation links ocean climate and ecosystem change. *Geophys. Res. Lett.*, 35, L08607, doi:10.1029/2007GL032838.

Durack P. J., and S. E. Wijffels, 2010. Fifty-year trends in global ocean salinities and their relationship to broad-scale warming. *J. Clim.*, 23, 4342–4362, doi: 10.1175/2010JCLI3377.1.

Emerson, S., S. Mecking, and J. Abell, 2001. The biological pump in the subtropical North Pacific Ocean: Nutrient sources,
420 Redfield ratios, and recent changes, *Global Biogeochem. Cycles*, 15(3), 535-554, 10.1029/2000GB001320.

Emerson, S., Y. W. Watanabe, T. Ono, and S. Mecking, 2004. Temporal trends in Apparent Oxygen Utilization in the upper pycnocline of the North Pacific: 1980-2000, *J. Oceanogr.*, 60(1), 139-147.

Franco, A. C., D. Ianson, T. Ross, R. C. Hamme, A. H. Monahan, J. R. Christian et al., 2021. Anthropogenic and climatic contributions to observed carbon system trends in the northeast Pacific, *Global Biogeochem. Cycles*, 35, e2020GB006829, https://doi. org/10.1029/2020GB006829.

Freeland, H., 2007. A short history of Ocean Station Papa and Line P, *Prog. in Oceanogr.*, *75*(2), 120–125, https://doi.org/10.1016/j. pocean.2007.08.005.

Friedlingstein, P., 2015. Carbon cycle feedbacks and future climate change, *Phil. Trans. R. Soc. A,* 373, 20140421, http://dx.doi.org/10.1098/rsta.2014.0421.

Good, S. A., M. J. Martin and N. A. Rayner, 2013. EN4: quality controlled ocean temperature and salinity profiles and monthly objective analyses with uncertainty estimates. *J. Geophys. Research Res.*, 118, 6704-6716, doi:10.1002/2013JC009067.

Gouretski, V., and R. Franco, 2010. On depth and temperature biases in bathythermograph data: Development of a new correction scheme based on analysis of a global ocean database. *Deep Sea Research Part I: Oceanographic Research Papers.* 57. 812-833. 10.1016/j.dsr.2010.03.011.

Heinze, C., S. Meyer, N. Goris, L. Anderson, R. Steinfeldt, N. Chang, C. Le Quéré, and D. C. E. Bakker, 2015. The ocean carbon sink – impacts, vulnerabilities and challenges. *Earth Syst. Dynam.*, 6, 327-358, doi:10.5194/esd-6-327-2015.

Helm, K. P., N. L. Bindoff, and J. A. Church, 2011. Observed decreases in oxygen content of the global ocean. *Geophys. Res. Lett.*, 38, L23602, doi:10.1029/ 2011GL049513.

Holte J., and L. Talley, 2009. A new algorithm for finding mixed layer depths with applications to Argo data and Subantarctic Mode Water formation. *J. Atmos. Oceanic Technol.*, 26, 1920–1939, doi: 10.1175/2009JTECHO543.1.

Huang, R. X., and B. Qiu, 1994. Three-dimensional structure of the wind driven circulation in the subtropical North Pacific. *J. Phys. Oceanogr.*, 24, 1608–1622.

Keeling, R. E., A. Körtzinger, and N.Gruber, 2010. Ocean deoxygenation in a warming world. *Annu. Rev. Mar. Sci.*, 2, 199–229, doi: 10.1146/annurev.marine. 010908.163855.

Kwon E.-Y., C. Deutsch, S.-P. Xie, S. Schmidtko, and Y.-K. Cho, 2016. The North Pacific Oxygen Uptake Rates over the Past Half Century. *J. Clim.*, 29, 61–76.

Mantua, N. J., S. R. Hare, Y. Zhang, J. M. Wallace, and R. C. Francis, 1997. A Pacific interdecadal climate oscillation with impacts on salmon production. *Bull. Am. Meteorolog. Soc.*, 78, 1069–1079.

McDougall T. J., and P. M. Barker, 2011. Getting started with TEOS-10 and the Gibbs Seawater (GSW) Oceanographic Toolbox, 28pp., SCOR/IAPSO WG127, ISBN 978-0-646-55621-5.

Mecking S., C. Langdon, R. A. Feely, C. L. Sabine, C. A. Deutsch, and D.-H. Min, 2008. Climate variability in the North Pacific thermocline diagnosed from oxygen measurements: An update based on the U.S. CLIVAR/CO2 Repeat Hydrography cruises, *Global Biogeochem. Cycles*, 22, GB3015, doi: 10.1029/2007GB003101.

Mecking, S., M. J. Warner, and J. L. Bullister, 2006. Temporal changes in pCFC-12 ages and AOU along two hydrographic sections in the eastern subtropical North Pacific. *Deep-Sea. Res. I*, 53, 169–187.

Melnichenko, O., P. Hacker, J. Potemra, T. Meissner, and F. Wentz, 2021. Aquarius/SMAP sea surface salinity optimum interpolation analysis, IPRC Technical Note No. 7, May 7, 2021.

Ono T., T. Midorikawa, Y. W. Watanabe, K. Tadokoro, and T. Saino, 2001. Temporal increases of phosphate and apparent oxygen utilization in the subsurface waters of western subarctic Pacific from 1968 to 1998. *Geophys. Res. Lett.*, 28(17), 3285-3288.

Osafune, S., and I. Yasuda, 2013. Remote impacts of the 18.6 year period modulation of localized tidal mixing in the North Pacific, *J. Geophys. Res. Oceans*, 118, 3128–3137, doi:10.1002/jgrc.20230.

Reynolds, R. W., T. M. Smith, C. Liu, D. B. Chelton, K. S. Casey and M. G. Schlax, 2007. Daily High-resolution Blended Analyses for sea surface temperature. *J. Clim.*, 20, 5473-5496.

Roemmich, D., 1983. Optimal estimation of hydrographic station data and derived fields, *J. Phys. Oceanogr.*, 13, 1544 – 1549, doi:10.1175/1520- 0485(1983)013<1544:OEOHSD>2.0.CO;2.

Ross, T., C. Du Preez, and D. Ianson, 2020. Rapid deep ocean deoxygenation and acidification threaten life on Northeast Pacific seamounts, *Glob. Change Biol.*, 6424–6444, https://doi.org/10.1111/gcb.15307

Sasano, D., Y. Takatani, N. Kosugi, T. Nakano, T. Midorikawa, and M. Ishii, 2015. Multidecadal trends of oxygen and their controlling factors in the western North Pacific, *Global Biogeochem. Cycles*, 29, 935–956, doi:10.1002/2014GB005065.

470   Sasano, D., Y. Takatani, N. Kosugi, T. Nakano, T. Midorikawa, and M. Ishii, 2018. Decline and bidecadal oscillations of dissolved oxygen in the Oyashio region and their propagation to the western North Pacific, *Global Biogeochem. Cycles*, 32, 909–931. https://doi.org/10.1029/2017GB005876.

Stramma, L., S. Schmidtko, S. J. Bograd, T. Ono, T. Ross, D. Sasano, and F. A. Whitney, 2020. Trends and decadal oscillations of oxygen and nutrients at 50 to 300 m depth in the equatorial and North Pacific, *Biogeosciences*, 17, 813–831,
475   https://doi.org/10.5194/bg-17-813-2020.

Takatani, Y., D. Sasano, T. Nakano, T. Midorikawa, and M. Ishii, 2012. Decrease of dissolved oxygen after the mid-1980s in the western North Pacific subtropical gyre along the 137°E repeat section, *Global Biogeochem. Cycles*, 26, GB2013, doi:10.1029/2011GB004227.

Talley, L. D., R. A. Feely, B. M. Sloyan, R. Wanninkhof, M. O. Baringer, J. L. Bullister, C. A. Carlson, S. C. Doney, R. A. Fine,
480   E. Firing, N. Gruber, D. A. Hansell, M. Ishii, G. C. Johnson, K. Katsumata, R. M. Key, M. Kramp, C. Langdon, A. M. Macdonald, J. T. Mathis, E. L. McDonagh, S. Mecking, F. J. Millero, C. W. Mordy, T. Nakano, W. M. Smethie, J. H. Swift, T. Tanhua, A. M. Thurnherr, M. J. Warner, and J.-Z. Zhang, 2016. Changes in ocean heat, carbon content and ventilation: Review of the first decade of global repeat hydrography (GO-SHIP), *Annual Review of Marine Sciences, 8,* 185-215, doi:10.1146/annurev-marine-052915-100829.

485   Trenberth, K. E., and J. W. Hurrell, 1994. Decadal atmosphere-ocean variations in the Pacific. *Climate Dynamics* 9, 303–319, https://doi.org/10.1007/BF00204745.

Uehara, H., A. A. Kruts, H. Mitsudera, T. Nakamura, Y. N. Volkov, and M. Wakatsuchi, 2014. Remotely propagating salinity anomaly varies the source of North Pacific ventilation, *Prog. Oceanogr.*, 126, 80-97, https://doi.org/10.1016/j.pocean.2014.04.016.

Ueno, H., and I. Yasuda, 2003. Intermediate water circulation in the North Pacific subarctic and northern subtropical regions, *J.*
490   *Geophys. Res.*, 108(C11), 3348, doi:10.1029/2002JC001372.

Watanabe, Y. W., T. Ono, A. Shimamoto, T. Sugimoto, M. Wakita, and S. Watanabe, 2001. Probability of a reduction in the formation rate of the subsurface water in the North Pacific during the 1980s and 1990s, *Geophys. Res. Lett.*, 28(17), 3289-3292, 10.1029/2001GL013212.

Whitney F. A., H. J. Freeland, and M. Robert, 2007. Decreasing oxygen levels in the interior waters of the subarctic Pacific.
495   *Prog. Oceanogr.*, 75(2), 179–199, doi: 10.1016/j.pocean.2007.08.007.

Yasuda I., S. Osafune, and H. Tatebe, 2006. Possible explanation linking 18.6-year period nodal tidal cycle with bi-decadal variations of ocean and climate in the North Pacific, *Geophys. Res. Lett.*, 33, L08606, doi:10.1029/2005GL025237.

Appendix A

500
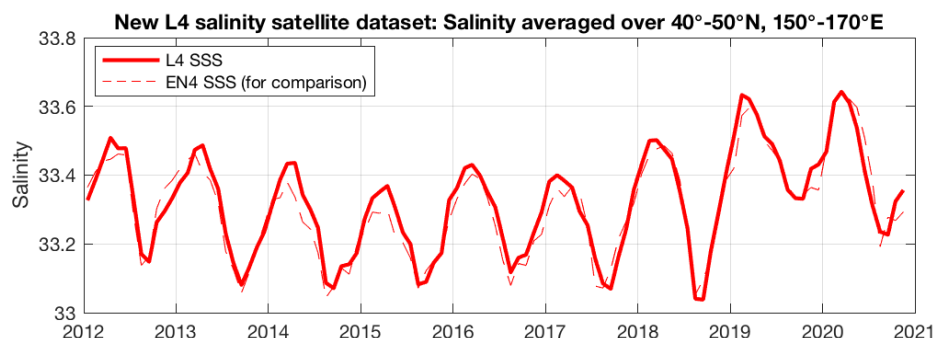
Figure A1. Satellite sea surface salinity (SSS) in the northwestern North Pacific averaged over 40–50°N, 150–170°E (see Figure 1a for area) using the new Multi-Mission Optimally Interpolated Sea Surface Salinity (OISSS) Level 4 V1.0 dataset (Melnichenko et al., 2021). Also shown are SSS averages from the EN4 dataset (dashed line) for comparison.

505
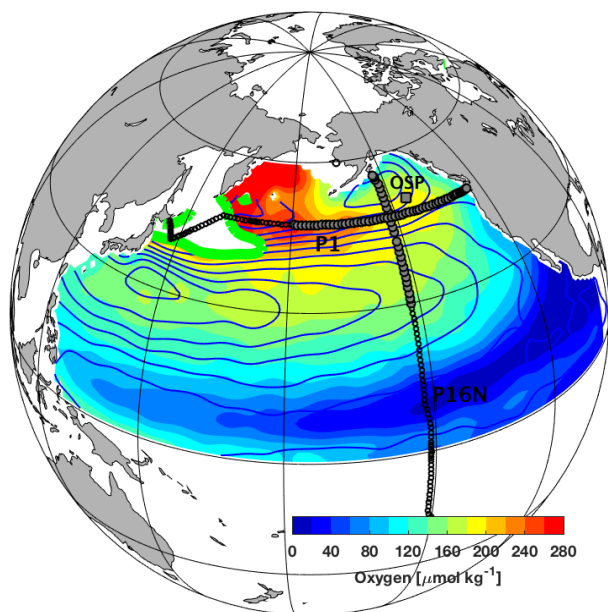
Figure A2. Dissolved oxygen (colored) on σ_θ=26.6 kg m^{-3} in the North Pacific. Blue contours mark streamlines (acceleration potential) on the
510   σ_θ=26.6 kg m^{-3} isopycnal, and light green contours mark the outcrop of this isopycnal in late winter (March). Oxygen decreases following streamlines because of respiration in the ocean interior. Data are from World Ocean Atlas and represent the climatological mean over six decades (Locarnini et al, 2013; Zweng et al., 2013; Garcia et al., 2014). In addition, circles mark station locations of the CLIVAR/GO-SHIP Repeat Hydrography cruises P16N and P1, with the larger gray-faced circles indicating the latitude and longitude ranges, respectively, of stations used for the difference plots in Figure A3. The location of Ocean Station P (OSP; Whitney et al., 2007) is marked by a gray square.

515

520

a)   b)
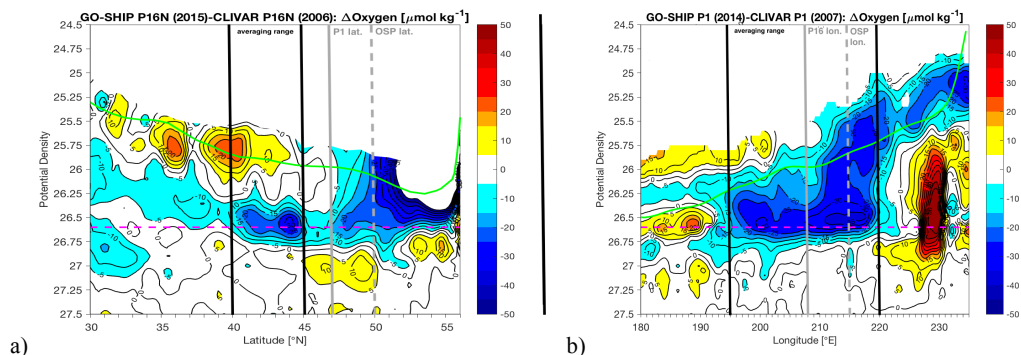
Figure A3. O₂ differences on potential density surfaces for portions of two North Pacific repeat hydrography sections collected as part of CLIVAR/GO-SHIP (a) along 152°W (P16N) – 2015 minus 2006, and (b) along 47°N (P1) – 2014 minus 2007. The location of the sections

525 relative to OSP is shown in Figure A2. Changes are calculated by objectively mapping the O₂ data from each repeat occupation to create latitude/longitude versus density grids and differencing the mapped data. The dashed magenta line in each panel marks the σ_θ=26.6 kg m⁻³ isopycnal. The light green lines mark the March mixed layer density along the sections, calculated from climatological data. The latitude and longitude of OSP are marked in panels (a) and (b), respectively, as dashed gray lines, and the latitude and longitude where P16N and P1 cross are marked in panels (a) and (b), respectively, as solid gray lines. The two black solid lines in each panel mark the averaging intervals used for

530 Figure A4. Note that the averaging interval in panel (a) (40-45°N) is somewhat to the south of the OSP latitude because this marks the region of largest O₂ decline on σ_θ=26.6 kg m⁻³ in the interior away from the mixed layer and matches the averaging interval used in previous work (Mecking et al., 2008).

535

a)   b)
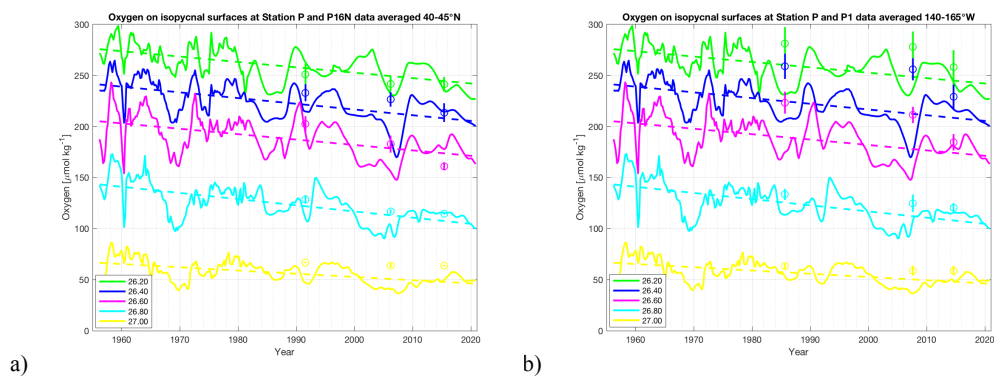
Figure A4. O₂ at OSP on isopycnals from σ_θ=26.2-27.0 kg m⁻³ (in 0.2 increments), including linear trends (dashed lines), as in Figure 3, together with averages on the same isopycnals from the WOCE (late 1980s/early 1990s), CLIVAR (2000s), and GO-SHIP (2010s) repeat hydrography

540 cruises, indicated by circles (mean) and vertical lines (standard deviation): (a) averages between 40-45°N for P16N cruises along 152°W in 1991, 2006, and 2015, and (b) averages between 140-165°W for P1 cruises in 1987, 2007, and 2014. The latitudinal (P16N) and longitudinal (P1) averaging intervals are shown by the black lines in Figures A3a and A3b, respectively.

545
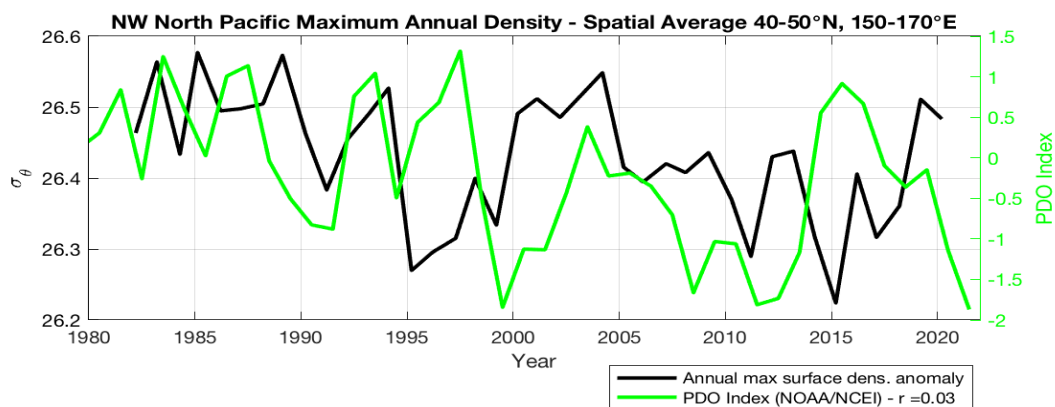
550

Figure A5. Annual maximum surface density anomaly in northwestern North Pacific (black; from Figure 6b) and annually averaged Pacific Decadal Oscillation (PDO) index (light green).

555
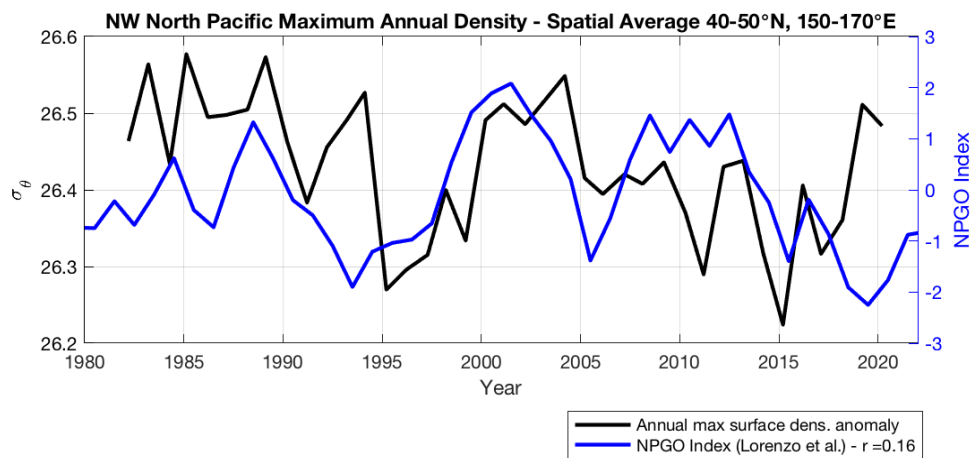
Figure A6. Annual maximum surface density anomaly in northwestern North Pacific (black; from Figure 6b) and annually averaged North
560 Pacific Gyre Oscillation (NPGO) index (blue).
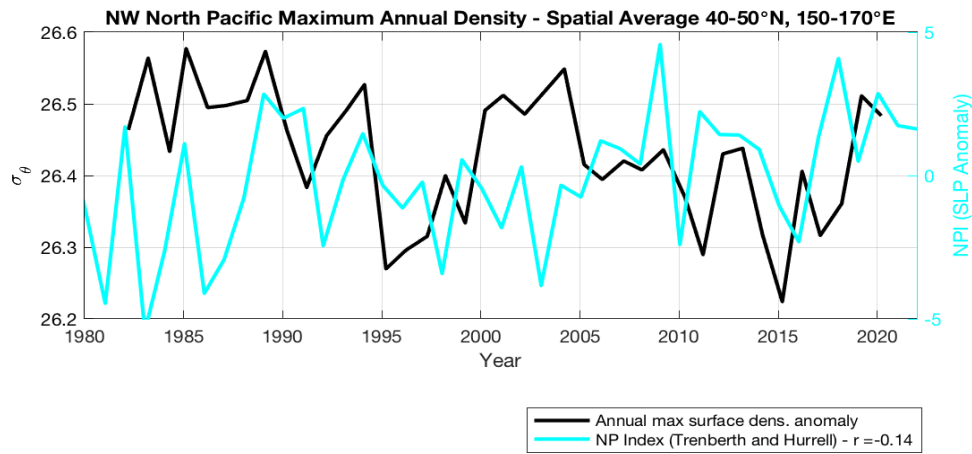
Figure A7. Annual maximum surface density anomaly in northwestern North Pacific (black; from Figure 6b) and annually averaged North
Pacific Index (NPI; cyan).